

# CFD CALCULATIONS OF WIRE WRAPPED FUEL BUNDLES: MODELING AND VALIDATION STRATEGIES

Ulrich Bieder, Valérie Barthel, Frederic Ducros, Partrick Quéméré, Simone Vandroux

*CEA-Grenoble, DEN/DER/SSTH/LDAL, 15 rue des Martyrs, F-38054 Grenoble*

## Abstract:

In the past, extensive numerical thermal-hydraulic investigations have been performed on the coolant of LMFBR fuel assemblies. These investigations have usually been limited to 7 to 19 pins and axially periodic boundary conditions due to the lack of available computer power. A generic investigation has been performed at CEA-Grenoble to develop a modeling and validation strategy in order to analyze the thermal-hydraulic behavior of full scale helical wrapped fuel bundles by using the Trio\_U<sup>1</sup> code. This strategy respects as far as possible the recommendations of Best Practice Guidelines (BPG) concerning the selection of appropriate physical and numerical models, the meshing procedure as well as sensitivity studies on the meshing and modeling. The proposed validation procedure has been focused on a correct prediction of the pressure distribution (not only the pressure drop) and of the velocity field within the fuel bundle as well as of the temperature distribution within the bundle.

## 1 INTRODUCTION

Fuel assemblies of liquid-metal fast breeder reactor (LMFBR) usually consist of wire-wrapped fuel pins in triangular arrangement. The fuel pins form sub channels in which the coolant circulates. The wire coils helically around each fuel pin and provides spacing between the fuel pins, increases the coolant mixing between the sub channels, and reduces the peak temperature as well as temperature gradient in the assembly. These desired effects of the wire spacer are compensated by an undesired increased pressure loss of the assembly.

Numerous experimental and numerical results are available on the flow behavior in wire spacer rod bundles. Hereby, the analyzed domain range from basic 7 pin bundles to realistic 61 or even 217 pin bundles and from simplified one wire pitch with axial periodic conditions to full scale assemblies. When analyzing the published data (e.g. Bubelis, 2008), the reader is rapidly lost in the quantity of experimental and numerical results which often do not converge to a common behavior and even contradict each other. Moreover, the published data rarely satisfy the quality demands for CFD validation.

At CEA-Grenoble a R&D project is under way to develop and validate numerical tools to analyze the performance of 4<sup>th</sup> generation LMFBR fuel assemblies. In this context, the prediction of the pressure loss of fuel assemblies as well as the prediction of possible hot spots on the pins surfaces, which limit the critical heat flux (CHF), needs both a reliable modeling strategy and a profound validation of the numerical approach. This approach and stepwise validation of the tool in order to qualify the modeling strategy is presented in this paper.

In Chapter 2, a brief characterization of the problem and a critical review of existing pressure loss correlations, which might be used for code validation, are presented. Different possibilities to achieve a good meshing are discussed in Chapter 3. The CFD reference code of the CEA, Trio\_U, is presented in Chapter 4 as well as the numerical model which was used for all calculations presented in this paper. Chapter 5 explains the procedure to validate the Trio\_U code for the application to rod bundles with wire spacers in Sodium cooled reactors. Finally, in Chapter 6, the validated model is applied to a full scale rod bundle of the PHÉNIX reactor, which has 61 pins and 9 wire-pitches.

---

<sup>1</sup> <http://www-trio-u.cea.fr>

## 2 CHARACTERIZATION OF THE PROBLEM

From a thermal hydraulic point of view, the helical spacer wires on the fuel pins are the origin of:

- A transversal flow which is an important mode of heat transfer and
- Secondary flows in the wake of the wires which increases the turbulence level.

Both effects improve on one hand the mixing in the fuel assembly (more homogeneous temperature distribution) and increase the pressure drop on the other hand. Both effects must be predicted correctly when analyzing the thermal hydraulic behavior of LMFBR fuel assemblies with numerical models.

### 2.1 Geometry

Figure 2.1 gives an overview over the geometrical complexity of a fuel assembly of the PHENIX reactor. The overall pressure drop of the assembly is defined by the individual pressure drops of the entry tube with the assembly base, the fuel zone with the 61 fuel pins and 9 pitches of the helical wire spacer, and the assembly head.

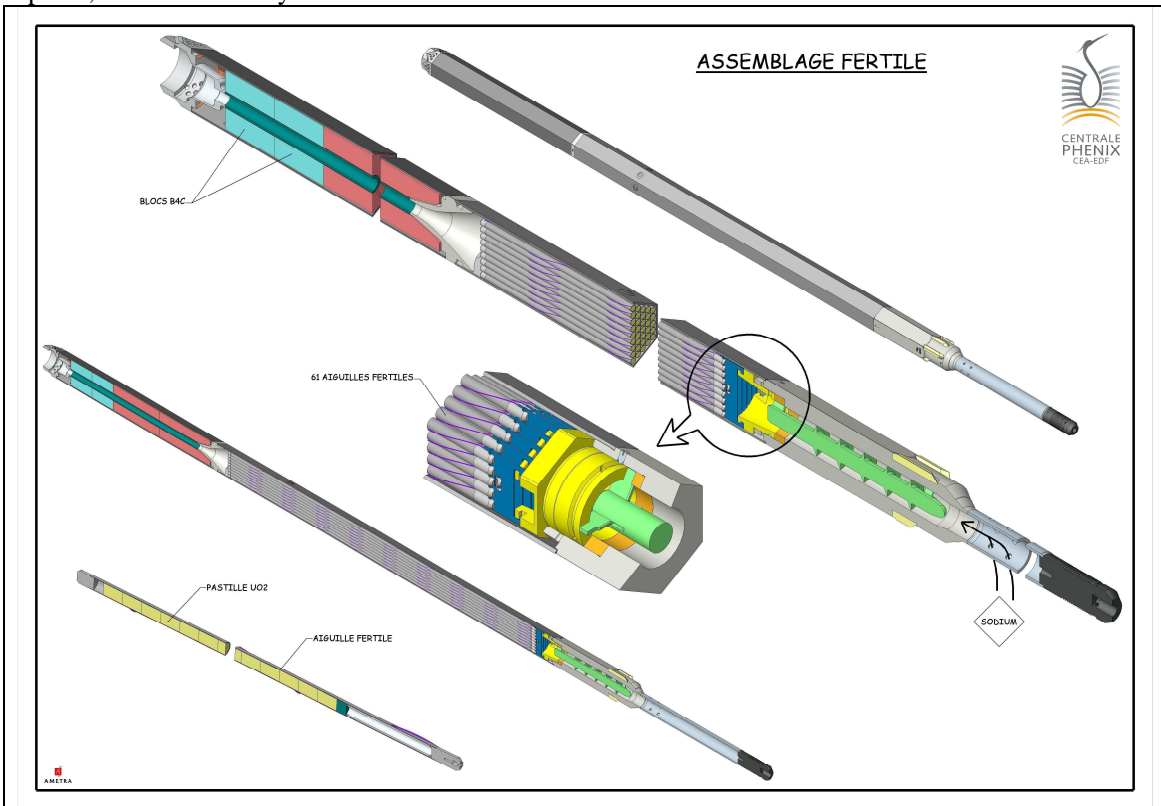


Fig. 2.1: Global view of an assembly of the PHENIX reactor

It is known that after about 1.5 wire pitches, the flow in the fuel zone is hydraulically well established. This justifies for a hydraulic analysis of the fuel zone the approximation of a periodic zone of the length of one pitch. As a matter of course, this approximation is not correct for thermal considerations since the temperature field in the assembly is developing axially along the whole assembly.

### 2.2 Pressure distribution

With  $\rho$  being the density and  $v$  the mean velocity of the coolant, the pressure loss due to the flow friction along a smooth pipe is calculated as:

$$\Delta P = f \cdot \left( \frac{L}{d_h} \right) \cdot 0.5 \cdot \rho \cdot v^2. \quad (2.1)$$

$L$  is the tube length and  $d_h$  the hydraulic diameter of the flow channel. For turbulent single phase flow the friction factor  $f$  can be estimated for many applications by using the Blasius formula as a function of the Reynolds number  $Re$ , namely:

$$f = 0.316 \cdot Re^{-0.25} \quad (2.2)$$

Bubelis (Bubelis et al., 2008) has published an evaluation of the existing wire wrapped fuel bundle friction factor/pressure drop correlations. In order to determine which friction factor correlation is most appropriate, the authors retraced the results of a large set of openly available experimental data on wire wrapped fuel assemblies and compared them to correlations which are incorporated in code SIM-ADS.

For a 19 pin experiment, performed in the ESTAIR test facility (Berthoux et al., 2008), Figure 2.2 shows the friction factors which are calculated for various correlations by SIM-ADS.

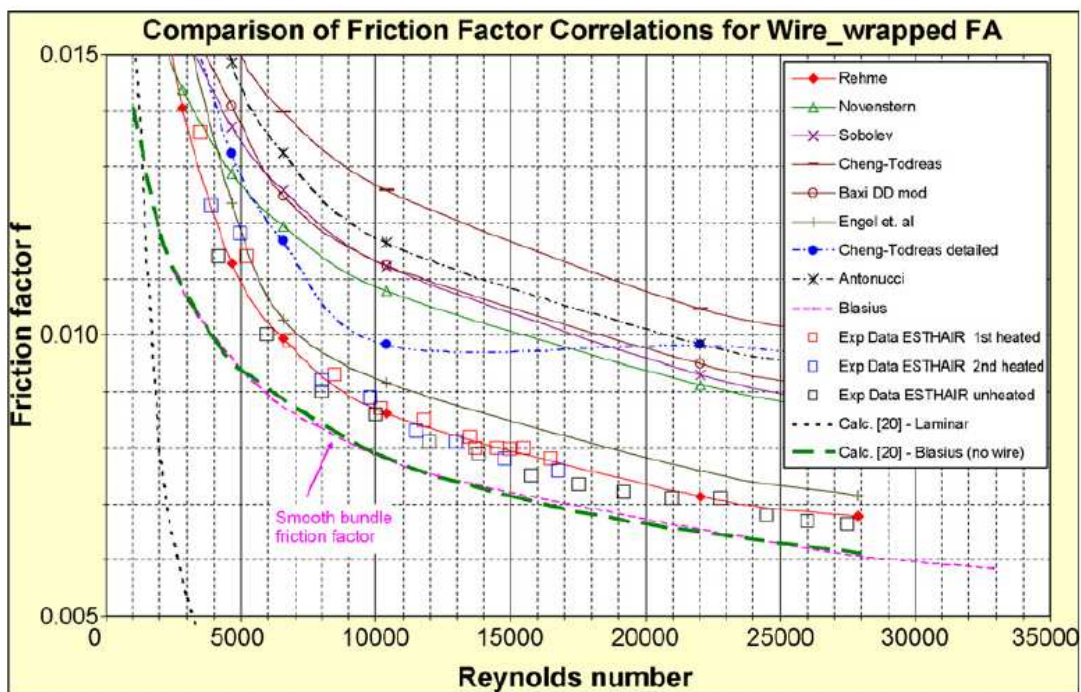


Fig. 2.2: Comparison of friction factor correlations to the ESTAIR experiment (Picture from Bubelis et al., 2008)

Friction factors calculated for the same Reynolds number vary up to 100% for different correlations although these correlations are widely used in pressure loss predictions. This wide range of “approved” correlations raises some questions:

- Each originally proposed correlation has been adapted to a specific experiment. Why do similar experimental setups lead to so different correlations?
- Some experimental configurations are well represented by many correlations. Why do the same correlations fail on other similar configurations?
- Assembled correlations promise to represent the majority of experiments. Is such a mean value over different experiments more justified than a correlation done under specific conditions?

- For the same Reynolds number, some authors (e.g. Bubilis et al., 2008) have proposed fluid dependant (air, water, sodium) correlations. What is the physical justification of such a proposal?
- Which experiment and correlation should code developers refer to for their model validation?

Further discrepancies exist also in the assessment of the same correlation done by different authors:

- Bubilis (Bubelis et al. 2008) proposed to use Rehme's correlation as a reference. This correlation represents most experiments. For some applications, the predicted friction factors are only about 5% above the lower limit of Blasius' law.
- Chun (Chun et al., 2001) concluded: "Rehme's correlation appears that it does not represent the effects of P/D (wire pitch to rod diameter) and H/D (wire length to rod diameter) well enough, and this correlation consistently under predicts the friction factor for overall flow regions".

As a consequence of the high bandwidth of results detected in published data, the authors of this paper have decided to rather analyze specific experiments with precisely defined boundary conditions for code validation than to hark back on general correlations. The direct contact between theoretician and experimenter has turned out to be essential for a successful numerical analysis of an experiment.

### **2.3 Temperature distribution and possible hot spots**

In the contact region between rod and spacer wire, the flow velocity is significantly reduced, in particular in the wake of the wire. At this location, the rod surface might locally heat up above the saturation temperature of the coolant. This might lead the evaporation of the coolant and create vapor bubbles which on their part can influence the neutron fluxes. This phenomenon is related to the critical heat flux (CHF), one of the limiting factors in all kind of nuclear reactors.

It is widely accepted that without a mixing device, the departure from nucleate boiling (DNB) occurs mainly on the central rod and there preferentially at the location facing azimuthally the adjacent rods. With a mixing device, generally the CHF is significantly higher; however the location of the DNB is dependent on many parameters as pressure and local mass velocity. It is thus of main interest to understand both, the global temperature distribution in the assembly and the possible occurrence of hot spots in the wake of the spacer wire. For this kind of application, unfortunately, only very limited experimental data are published to date for code validation.

## **3 MESHING OF THE CALCULATION DOMAIN**

### **3.1 Hexa- or tetra/poly meshes**

The flow in fuel assemblies consists primarily of a directional flow in axial direction with a superposed secondary flow in the sub-channels. This main flow is disturbed by the presence of the spacer wire which on one hand forces the flow to follow locally the direction of the wire rotation and on the other hand creates a secondary flow in the wake of the wire. A hexagonal mesh which follows globally the rotation of the wire can impose a non physical global rotation of the flow due to the fact that the flow tends to follow the mesh. Further, the geometrical complexity can lead to highly deformed hexahedral meshes, especially in areas where the wire spacer approaches the adjacent pin. In order to avoid these problems, most of the recently performed numerical analysis has been done on either tetrahedral or polyhedral meshes (e.g. Gajapathy et al., 2009, Raza et al., 2008 and Hamman et al., 2010).

### **3.2 Imperfectly large meshes**

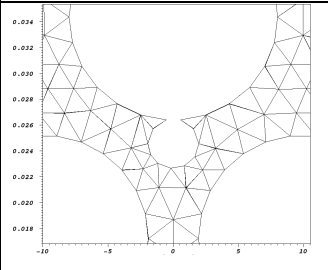
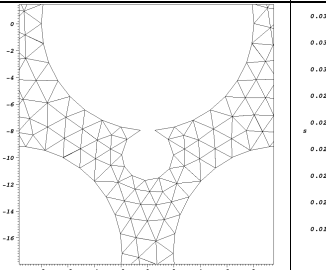
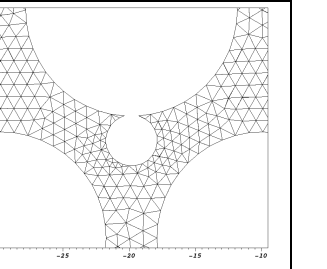
Calculations with meshes which do *not* respect standard recommendations of Best Practice Guidelines (BPG) (e.g. Mahafy et al., 2007) can nevertheless lead to realistic pressure losses. When creating large meshes near solid walls and applying wall functions, the whole physics of the problem is imposed by the wall function. Hence, the pressure drop can be close to Blasius's correlation, which describes the pressure loss in fully turbulent channels. This can easily lead to the wrong conclusion that a modeling

approach is validated although the approach does not respect the slightest requirements for a CFD calculation. In this context it is important to note that the friction factor of the correlation of Rehme is for some applications only 5% higher than that of the correlation of Blasius (see chapter 2.2).

### 3.3 Mesh refinement

The effect of the mesh refinement was tested with the Trio\_U code on an ESTAIR experiment (Berthoux et al., 2008). The friction factor of various correlations applied to this experiment is given in Figure 2.2. The pressure losses, calculated for  $Re=17479$  and different mesh refinements, are given in Table 3.1.

Table 3.1: Pressure loss for an ESTAIR experiment: Function of the mesh refinement

Turbulence Model	k-ε	k-ε	k-ε
Mesh refinement			
Nb of points between rods	5	7	11
Pressure loss	1160 m <sup>2</sup> /s	1185 m <sup>2</sup> /s	1200 m <sup>2</sup> /s
Difference to ESTAIR	20 %	22 %	23 %

One wire pitch was simulated and periodic axial boundaries are used. The numerical model is described with more details in Chapter 4.2. The calculated pressure loss which corresponds to the term  $1/\rho \Delta P/\Delta x$  are compared in Table 3.1 to the experimental pressure loss of 970 m<sup>2</sup>/s. A mesh convergence can be found for a mesh refinement of at least seven calculation points between the rods. The significant over prediction of the pressure loss is probably related to the use of the k-ε turbulence model (see chapter 4.1). It is important to note that, although the calculation with the largest meshes lead to the best comparison to the experiment, the application of this mesh refinement is to avoid since basic recommendations of BPG (e.g. Mahaffy et al. 2007) are violated!

In recent publications, unstructured meshes are used with mesh refinements of about 60,000 tetrahedrons (Raza (2008)) to 8 Million polyhedrons (Hamman (2010)) per rod and wire pitch. The number of meshes signifies in this context also calculation points, for in the used commercial codes, mesh centered discretization schemes are used. In the presented Trio\_U calculations, generally 150,000 tetrahedrons per rod and wire pitch were used to get mesh independent results. This refinement corresponds to about 300,000 calculation points per rod and wire pitch (face centered discretization).

### 3.4 Axial expansion of the tetrahedral meshes

The meshes have been generated with commercial mesh generators. The tetrahedral cells of the meshing can be expanded in flow direction in order to reduce the total mesh number. However, a too strong one-directional degradation of the tetrahedrons can also degenerate the accuracy of the calculation. To achieve an axial mesh expansion, the CAD model is compressed in flow direction before meshing. Then, after the meshing, the resulting mesh is decompressed in flow direction by the same factor. Although expansion factors up to eight did not show a significant change of the pressure drop, a factor four has been used in most calculations presented here.

### 3.5 Modeling of the wire spaces

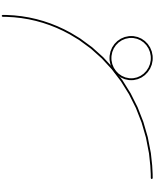
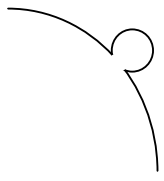
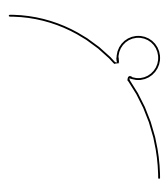
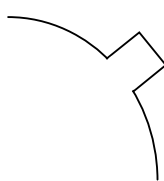
The helically wrapped spacer wire has different tasks to perform:

- To prevent a horizontal displacement of the fuel rods,
- To suppress vibrations and
- Acts as a mixing device which reduces in the assembly:
  - The temperature gradients and
  - The critical heat flux.

These desired effects are bought by an increased pressure loss. In the wake of the wire, in locations with low fluid velocities, increased rod surface temperatures can form. Therefore, the modeling of the wire should allow the formation of both realistic hot regions in the vicinity of the wire and correct axial pressure drops. In order to insure such a correct modeling the meshes in the contact region between wire and rod should not sustain a degradation of the mesh quality.

Table 3.2 shows four fundamentally different options to model the spacer wire. Remarks on potential meshing restrictions and on the possibility to predict hot spots are added to the Table for each wire form. When the wire is modified, it is difficult to conserve both the cross section and the wetted perimeter of the wire, which play an important role in the pressure loss.

Table 3.2: Comparison of various approaches used to model the wire spacer

Contact between the rod and the wire	Characterization	Meshing	Temperature in contact zone
	Reality	Almost impossible to mesh due to tangencies	Can be calculated correctly
	Radial displacement of the circular wire into the rod for about 5% of the wire diameter	Homogeneous meshing with only some degraded tetrahedrons	Possible hotspots between rod and wire can be predicted.
	Blending which can be degraded to large radii (so called open wires)	Very small meshes in the contact zone might be created	Possible hotspots between rod and wire can be predicted with some uncertainty.
	Square wire of equivalent surface as the wire	Easy to mesh	Possible hotspots between rod and wire can not be predicted

Calculations with the Trio\_U code have shown an increased pressure loss for square wires of up to 5% compared to a displaced wire. Hamman (Hamman et al., 2010) has shown that open wires can increase the pressure drop by up to 15%, depending on the rod/wire contact form. As shown by Raza (Raza et al., 2008), hexagonal forms of the wire as well as rhombi also overestimate the pressure drop in the assembly of 16% and 19%, respectively, compared to calculations with open wires.

As a conclusion it seems that the displacement of the circular wire into the rod of about 5% of the wire diameter might be an acceptable compromise to model the wire. This technique has also been applied successfully by Gajapathy and Hamman (Gajapathy et al., 2007, Hamman et al., 2010).

## 4 THE NUMERICAL MODEL

### 4.1 Turbulence Modeling

Most of the numerical investigations have been done with the k- $\epsilon$  turbulence model and logarithmic wall functions. This modeling seems to overestimate the pressure loss. This is particularly true when the Rehme correlation (see Bubelis et al. 2008) is taken as a reference. The overestimation of the friction factor, calculated recently by Gajapathy (2007) and Raza (2008), is shown in Table 4.1. The corresponding correlations used by the authors for model verification are added to the Table.

Table 4.1: Predicted friction factors by using a k- $\epsilon$  turbulence model

Reference	Reynolds number	Friction Factor Calculated	Friction factor Correlation and Correlation
Trio_U	17479	0.0086	0.0070 / Rehme
Gajapathy (2008)	10000	0.0107	0.0099 / Novendstern
	50000	0.0072	0.0063 / Novendstern
Raza (2008)	56000	0.046	0.0300 / Cheng&Todereas

This observed overestimation is in accordance to the conclusion of Hamman et al. (2010): “The realizable k- $\epsilon$  turbulence model agreed well with data produced using Novendstern’s empirical correlation, while the SST (Menter) k- $\omega$  turbulence model showed good agreement with Rehme’s empirical correlation”.

### 4.2 Trio\_U code

Trio\_U (Trio\_U, 2010) is a thermal-hydraulic code for strongly instationary low Mach number, turbulent flows. The code is especially designed for industrial CFD calculations on structured and non-structured grids of several tens of millions of nodes (Ducros et al., 2010). The platform independent code is developed at the CEA-Grenoble. It is based on an object oriented, intrinsically parallel approach and is coded in C++ language. The flexible code structure allows the user to choose a suitable discretization method and to combine various appropriate physical models, including different treatments of turbulence. Several convection and time marching schemes as well as a wide range of boundary conditions are available. This flexibility is implemented for massively parallel computing without a significant reduction of the overall performance of the code.

For unstructured grids, the hybrid « Finite Volume based Finite Element » method (VEF) is applied. This method consists in determining for a continuous problem a discrete solution in the space of the finite element by maintaining the balance notation of finite volumes. The space discretization is performed on triangles in 2-dimensional cases and on tetrahedral cells in 3-dimensional cases. In Trio\_U, the main unknown velocity and temperature are located in the centre of the faces of an element (triangle or tetrahedron). The pressure however is discretized in the centre and in the vertices of the element (staggered mesh) in order to improve the velocity/pressure coupling.

The following numerical scheme was used in the simulation presented in this paper. More information on the code and the discretization can be found in Ducros et al. 2010.

Table 4.2: Assembly of the numerical model to simulate the flow around helical wire spacers

Meshing	Tetrahedrons	<ul style="list-style-type: none"> <li>○ At least 7 calculation point between pins</li> <li>○ Radial displacement of the circular wire into the rod for about 5% of the wire diameter</li> <li>○ Expansion factor of four of the tetrahedrons in axial direction</li> </ul>
Discretization	Finite Volume Elements	P0/P1 for : <ul style="list-style-type: none"> <li>○ Pressure</li> </ul> P1-non conform for : <ul style="list-style-type: none"> <li>○ Velocity</li> <li>○ Temperature</li> <li>○ K and <math>\epsilon</math></li> </ul>
Time scheme:		Euler implicit First order backward
Navier-Stokes equations	Convection	Ef_stab
	Diffusion	centered
	Presser solver	GCP, SSOR preconditioning
	Thermal effects	Boussinesq's hypothesis ( $\Delta\rho/\rho < 0.1$ )
	Wall treatment	Wall law « Reichardt » $y^+ > 40$
Turbulence modeling	Approach	Boussinesq's hypothesis with turbulent viscosity ( $\nu_t$ )
	Turbulence model	RANS type k- $\epsilon$
	Convection of k et $\epsilon$	Ef_stab
	Diffusion of k et $\epsilon$	Centered
	Thermal effects	An-isotherm terms
	Wall treatment	Equilibrium wall laws
Energy equation	Convection of Temperature	Ef_stab
	Diffusion de la Temperature	Centered
	Wall treatment	Wall law « Kader »
	Treatment de la turbulence	Turbulent Pr
Conservation of masse	Incompressible fluid $\text{div}(u)=0$	Pressure projection method

## 5 VALIDATION OF THE MODEL

The qualification of the modeling methodology implies three elementary steps (Bieder et al. 2008), one verification and two validation steps:

- verification (solving the equations right, what is usually done by code developers),
- validation (solving the right equation)
  - elemental (separate effect studies) and
  - integral (coupled multiple effect studies and benchmarks)

The qualified model can then be applied to the real, full scale geometry by using the same modeling methodology which was developed during the qualification process. The validation process for Sodium cooled reactor applications is performed here in three successive steps with increasing complexity of the associated physics by simulating:



- Boundary layers on solid wall in straight tubes (Helium test),
- Pressure losses and flow fields in wire wrapped rod bundles (Water test),
- Temperature distribution in heated rod bundles without wire spacer (Sodium test).

It is mandatory that the same modeling strategy is applied in each validation step.

### 5.1 Flow in straight tubes

In industrial applications it is often not possible to follow in detail all requirements of BPG (Mahaffy et al. 2007). Concerning the geometry, this is related to the complexity of the topology of the calculation domain and to the available computer power which prevents the use of a perfectly adapted meshing. In the context of wire wrapped fuel bundles it is mandatory to verify the correct modeling of hydraulic and thermal boundary layers on solid walls when mesh sizes are used which are similar to those presented in Chapter 3.3.

For this purpose, a periodic turbulent channel flow at  $Re=10^5$  (Helium at 70bar and 273K) with heat transfer is analyzed with two mesh refinements:

- A reference meshing which is based on the application of BPG;
- An industrial meshing which is close to the mesh refinement proposed Chapter 3.3.

Both meshes are presented in Figure 5.1. Axially only two layers of tetra meshes are generated. A laminar flow profile with a mean velocity of 0.655m/s and at temperature of 0°C is used as initial condition. A constant heat flux of 1000 W/m<sup>2</sup> is imposed at the tube wall. The turbulence is modeled by a k-ε model with logarithmic wall functions. Constant physical properties are used and thermal feedback effects on the flow are neglected.

Since the constant wall heat flux heats up a flow of constant mass flow rate, the mean temperature in a tube cross section increases linearly in time. Hydraulic convergence is achieved after 300s. Taking the center velocity as a reference this time span corresponds to a fictive tube length of about 150 times the diameter. The resulting temperature distribution in the tube is given in Figure 5.2 at 600s.

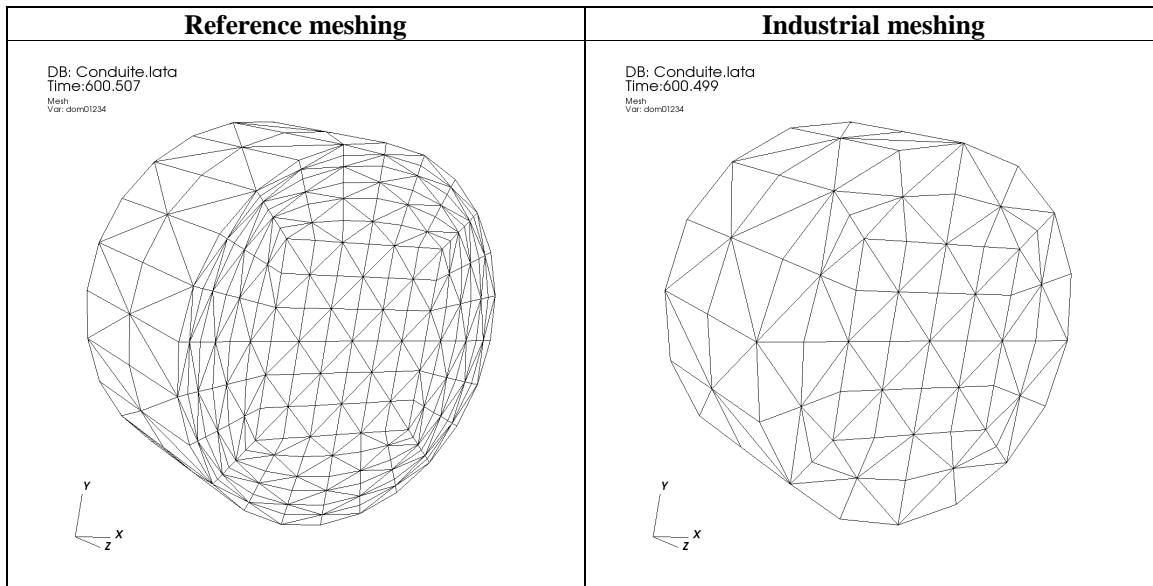


Fig. 5.1: Two mesh refinements for the same application in different situations

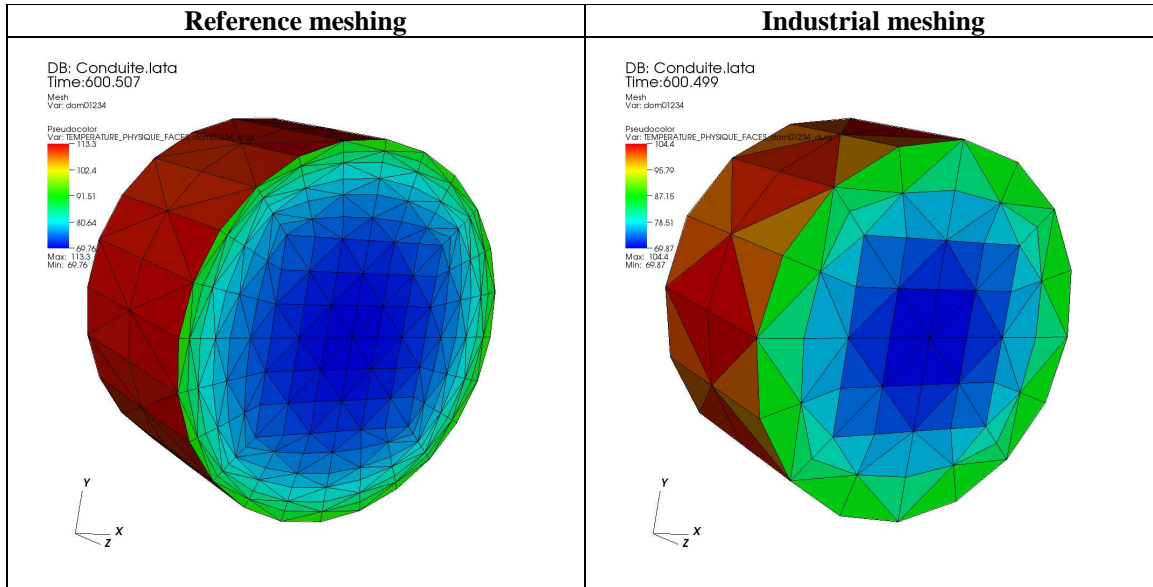


Figure 5.2: Temperature distribution in the periodic tube after 600s

Moreover, as also shown in Table 5.1, the friction velocity and the pressure loss are very similar for both meshes. Extrapolating the result with the industrial meshing to tube bundles, it seems that a simulation with mesh convergence in the hydraulic part underestimates the wall temperature. Although this is against the rule of conservative assumptions for nuclear safety analysis, an error of 10% to 15% in the prediction of wall temperatures seems to be acceptable for many industrial applications.

Table 5.1: Periodic tube flow: Quantitative comparison of the results of two meshes

	Theoretical values	Reference meshing	Industrial meshing
Bulk velocity [m/s]	0.655	0.655	0.664
Friction velocity [m/s]	0.0309 (Blasius)	0.0317	0.0321
Pressure loss [Pa]	0.0019 (Colebrook)	0.0020	0.00206
Wall temperature [°C]	114.5	112.17	101.88

## 5.2 Flow in rod bundles

### 5.2.1 The hydraulic Lafay experiment

A simple pressure loss comparison, as shown in Table 3.1 for meshing purpose, is not sufficient for code validation. Unfortunately, only limited published experimental data exist on local pressure field measurements (e.g. Fernandez et al., 2000) and local velocity measurements in order to improve the knowledge of the fine flow structures in the flow sub channels of the tube bundle. The authors still consider the results of the 19 pin water experiment performed at CEA in 1975 (Lafay et al., 1975) as high quality data.

#### a) Setup of the experiment

The mockup consists of glass rods placed in a hexagonal housing. Three faces of the hexagonal tube were transparent. In these experiments static pressure traps were connected to differential manometers at various locations in the hexagonal stainless steel walls. The movement of the fluid was observed through the transparent faces using fine bubble visualization technique. The top view of the experimental device and the locations of the pressure measurements in the hexagonal stainless steel wall (rectangular sub channel) are given in Figure 5.3. The geometrical specifications of the experimental set up and the corresponding CAD model as well as the condition of the simulation

presented here are given in Table 5.2. Only one wire pitch with periodic axial boundary conditions was modeled.

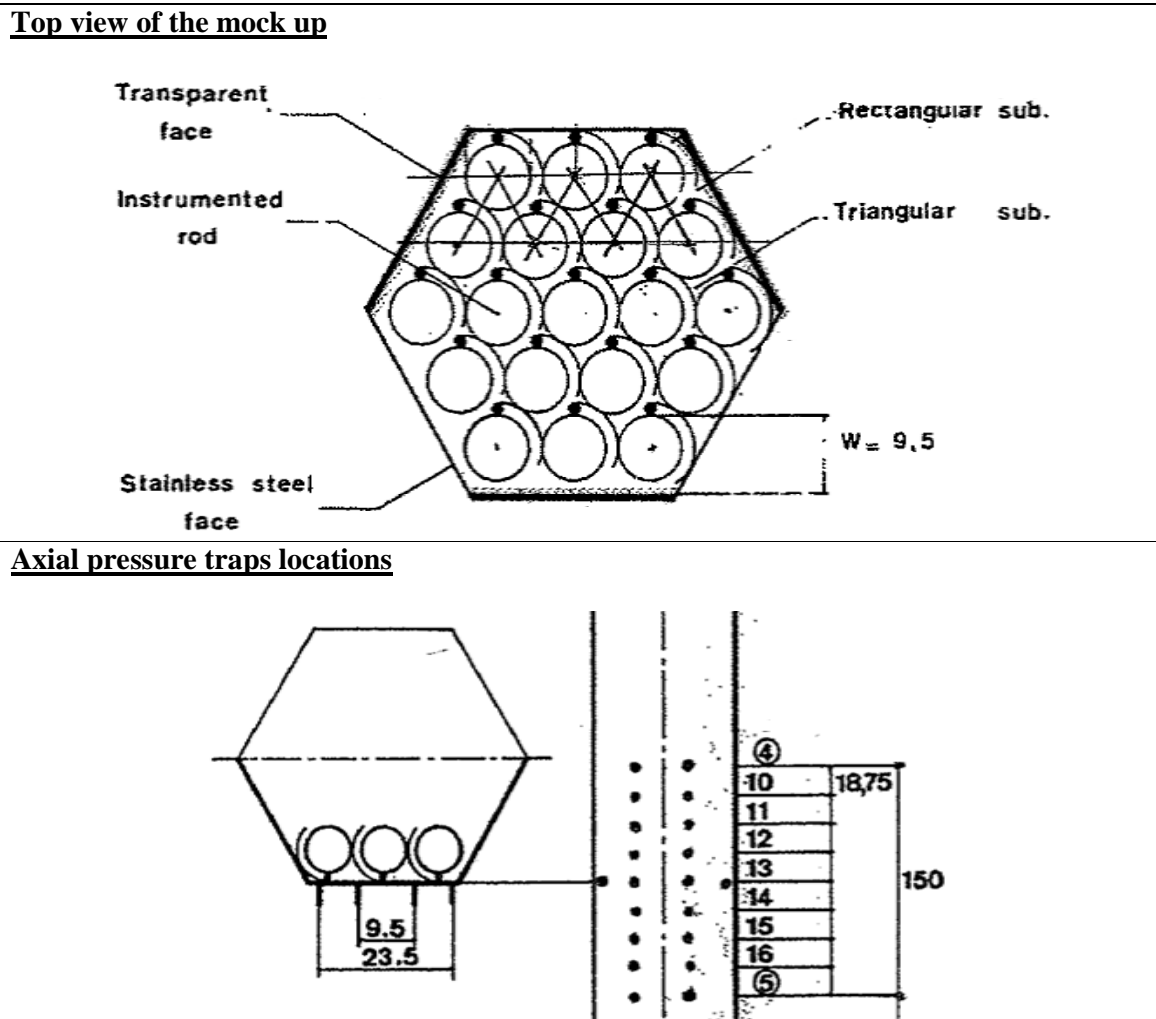
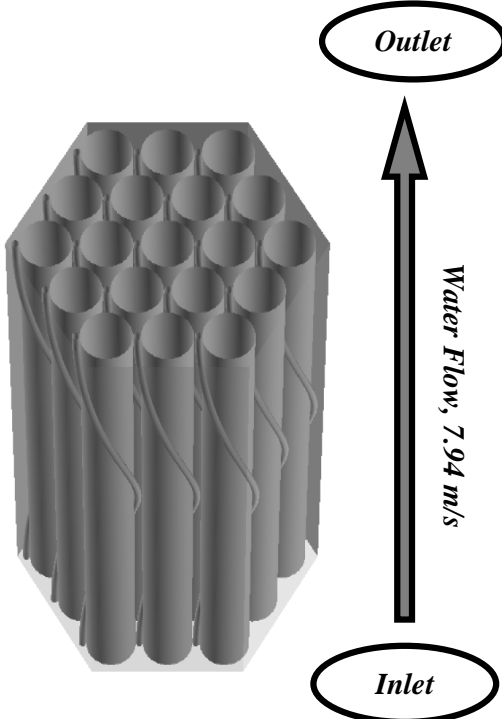


Figure 5.3: The setup of the Lafay experiment

As for the ESTAIR experiment (Chapter 3.2), numerical test calculations with the Trio\_U code have shown that mesh independent results can be obtained when at least seven calculation points are located between two rods. This mesh refinement leads for the simulation of the Lafay experiment to a mesh of about 3 Million tetrahedrons (6 Million calculation points for the used discretization) when using an axial expansion factor of four. The modeling strategy involves further the application of the numerical model described in chapter 4.2 and the treatment of boundary layers with industrial meshes as described in chapter 5.1.

Table 5.2: Specification of the Lafay experiment (geometry and experimental condition)

<u>Specification of the Subassembly</u>	
Number of Pins	19
Diameter of Pin	8.00 [mm]
Pin Array Pitch	9.50 [mm]
Diameter of Spacer Wire	1.32 [mm]
Total Length of Pin	810 [mm]
Wire-wrapping Pitch	150 [mm]
<u>Experimental Conditions</u>	
Flow Rate	795 [g/s/m <sup>2</sup> ]
Inlet Temperature	20 [°C]
Average Velocity	7.94 [m/s]
Reynolds Number	30 000



### b) The axial pressure distribution

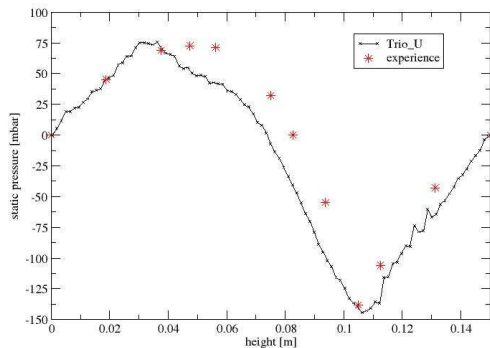


Fig. 5.4: Axial pressure distribution in the Lafay experiment

Figure 5.4 shows the axial static pressure distribution on the peripheral hexagonal wall (rectangular sub channel) of the fourth wire pitch. The mean pressure gradient of 2.6 bar/m is subtracted from the axial profile. This gradient is identical for both experiment and calculation. Since wires of small diameters produce a less important wake than wires of large diameters, it seems that the configuration of the Lafay experiment can be better represented by the  $k-\epsilon$  model than the ESTAIR configuration (see Table 3.1).

The comparison of this reduced pressure between experiment and calculation shows a good accordance. The highest pressure difference shown in Figure 5.4 between

maximum and minimum pressure can reach 70 % of the mean axial pressure drop of one pitch.

### c) Azimuthal pressure distribution

On Figure 5.5 the transverse static pressure around the complete hexagonal duct at the same axial location has been plotted versus the side length. On the left side, the experimenters have plotted a continuous line in the experimental values. The notation of the faces is also given on this side. On the right side, the experimental values (stars) are compared to the calculated values (line). The values of the experiment and the calculation are in good accordance. Minimum and maximum of the pressure

are obtained on both sides of the face where the wire is in the peripheral gap. This azimuthal pressure difference represents 64% of the pressure drop of the axial pressure drop of one wire pitch.

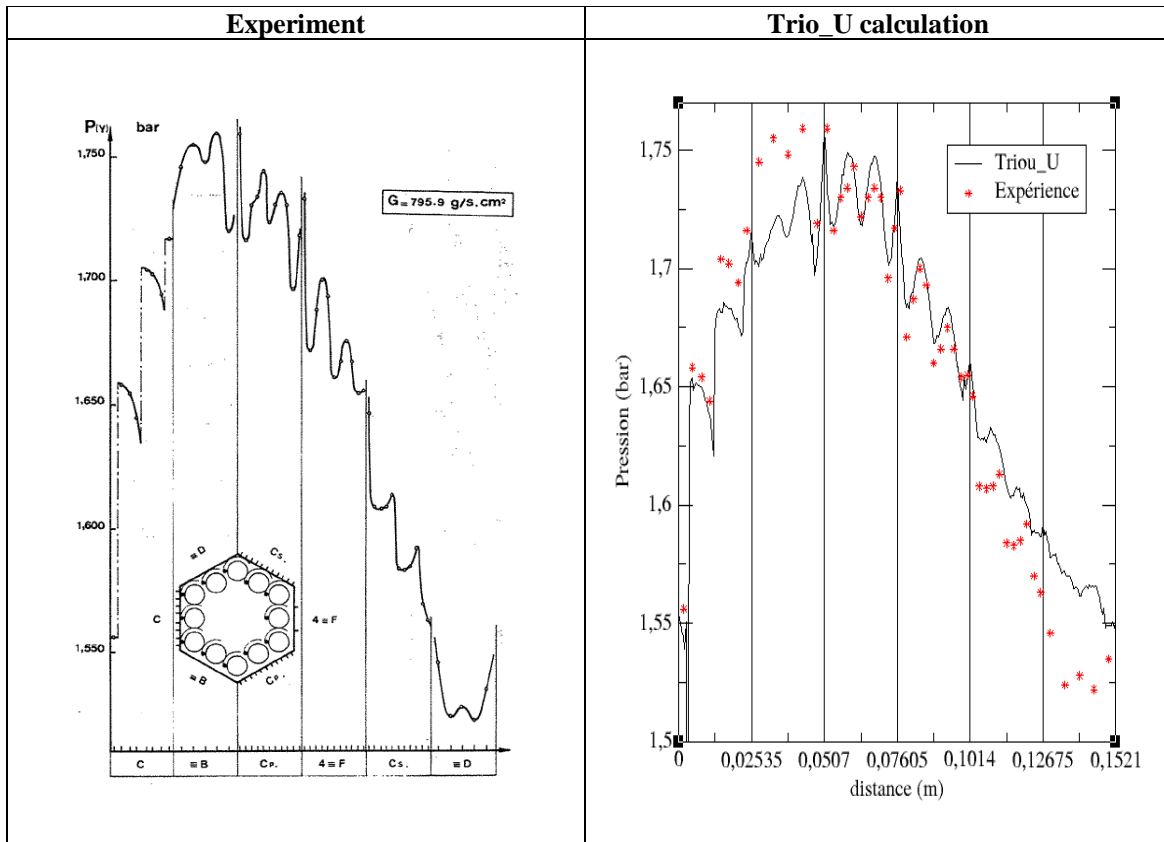


Fig. 5.5: Azimuthal static pressure distribution in the hexagonal duct in one elevation

#### d) Peripheral velocity distribution

Figure 5.6 shows on the left a typical flow pattern observed experimentally through one transparent face of the hexagonal tube. A clear movement of the fluid in the peripheral channel is induced by the helical wire in the direction of the wire rotation. This swirl flow is periodic with axial direction and is a function of the wire position.

The analysis of fine bubble photographs have shown that the peripheral velocity vectors angles are not the same as the wire wrap angles and depend on the wire position. The highest swirl velocities of about 48% of the local axial velocity are detected for the position 16 (the axial location is given on Figure 5.3). The lowest swirl velocities of 6% to 13% of the local axial velocity are detected approximately for the position 12. These features of the flow are represented qualitatively by the Trio\_U calculation (right side of Figure 5.6).

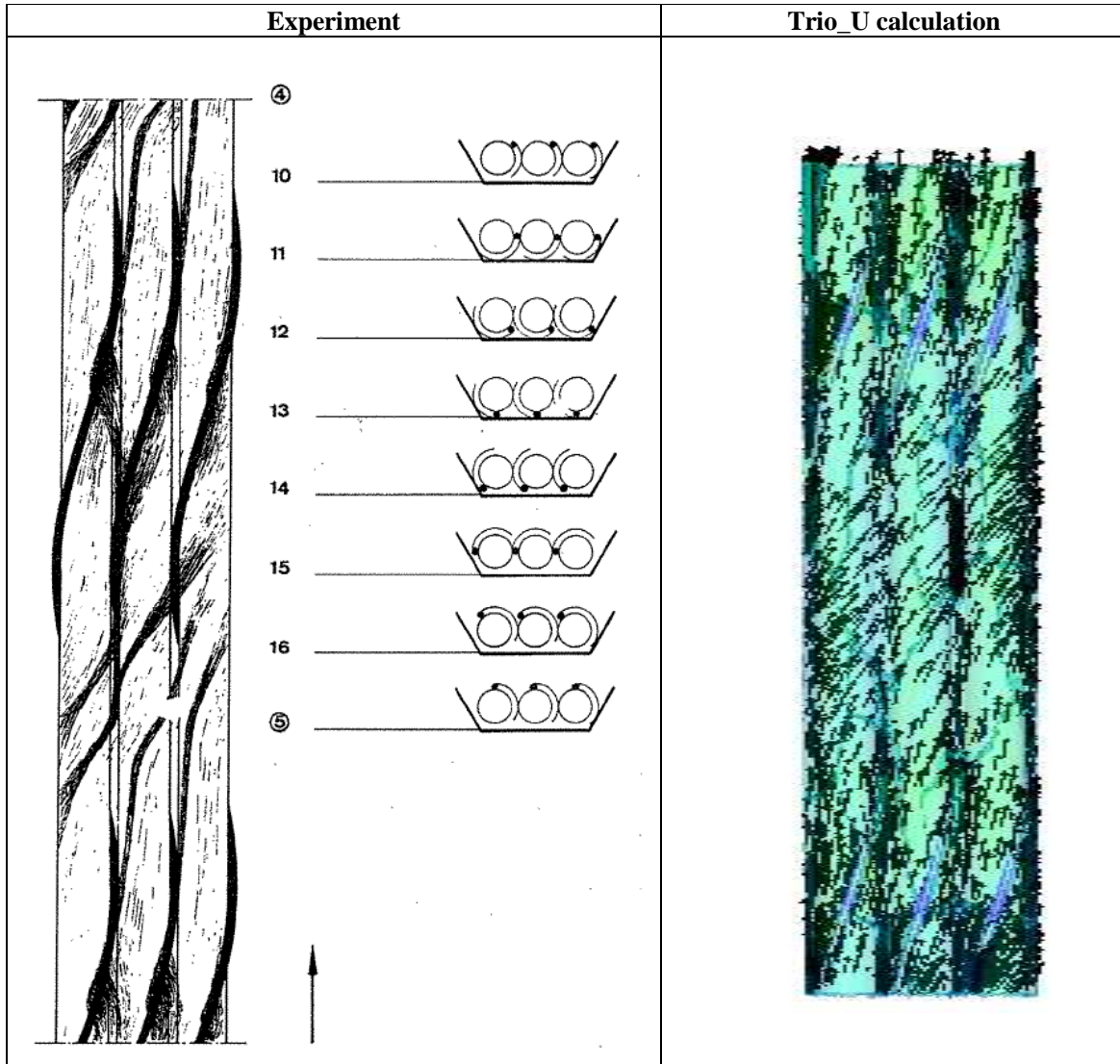


Fig. 5.6: Qualitative comparison of the velocity vectors near a transparent face of the duct

### 5.2.2 The thermal-hydraulic GR16 experiment

Sodium experiments on core thermal-hydraulics in tube assemblies with spacer wires, which can be used for code validation, have not been published to date (Smith et al. 2008). However, the heat exchange in tube bundles without spacer wire has been investigated in the framework of the French program of thermal-hydraulics on Sodium/Sodium heat exchangers (Bertoux et al., 1992, Berthoux, 1995). The GR16 test facility of the CEA-Grenoble simulates the heat transfer within a 4x4 vertically arranged and electrically heated rod bundle ( $d=18.7$  mm) which is placed non-centered in a rectangular container (see Figure 5.7 and Table 5.3). Detailed temperature measurements were performed at four levels (Z0 to Z1) in the upward Sodium flow as well as on the surfaces of the rod and container walls. For the level Z0, spatially highly resolved temperature profiles in x direction were measured with a mobile device in the central sub-channels along the lines of  $y=0.001275$ m,  $y=0.003825$  and  $y=0.006375$ m. The temperature profiles in x direction at  $y=0$ m were measured at the levels Z1, Z2 and Z3.

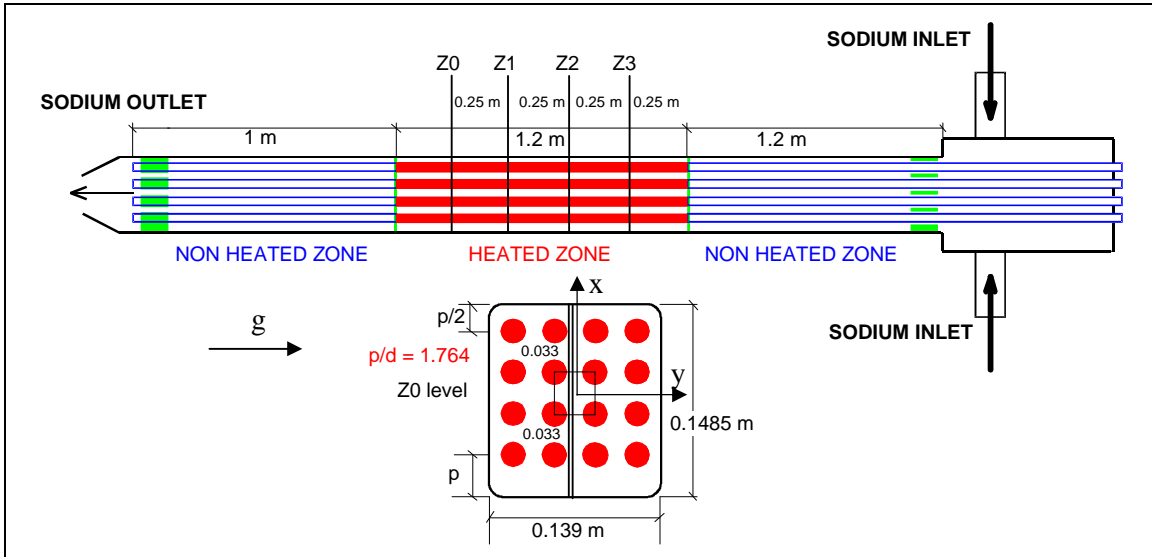
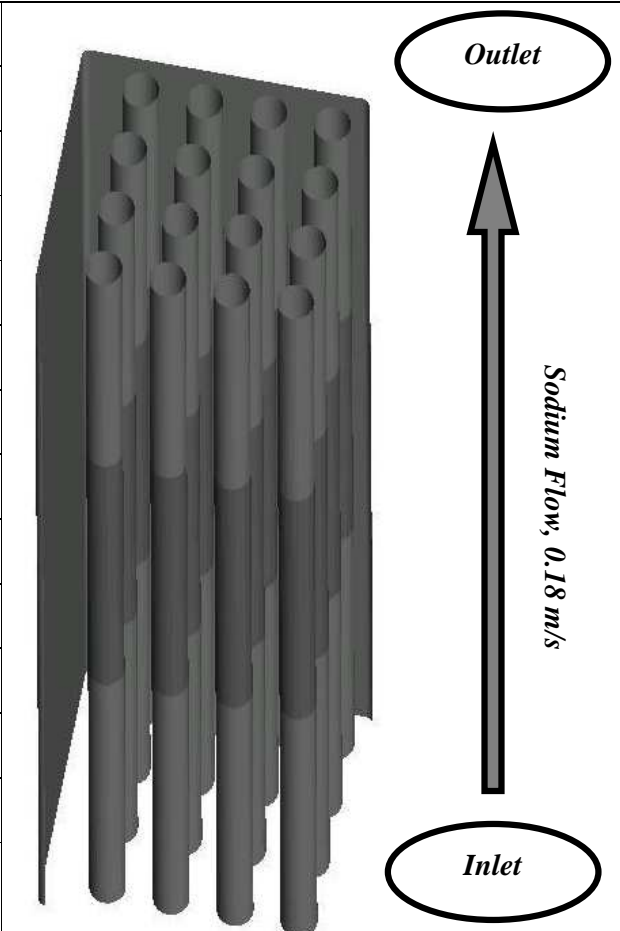


Fig. 5.7: Vertical cross section through the GR16 experimental setup

Table 5.3: Characterization of the analyzed experiment

<b><u>Specification of the Subassembly</u></b>	
Number of Pins	16
Diameter of Pin	18.7 [mm]
Pin Array Pitch	33 [mm]
Diameter of Spacer Wire	- [mm]
Total Length of Pin	3400 [mm]
Length of Heated Region	1200 [mm]
Wire-wrapping Pitch	- [mm]
<b><u>Experimental Conditions</u></b>	
Flow Rate	2.77 [l/s]
Total Power	300 [kW]
Inlet Temperature	302.4 [°C]
Average Velocity	0.017 [m/s]
Reynolds Number	20 200



The thermal hydraulics of the flow in the whole bundle (total length of 3.4m) has been simulated with the Trio\_U code without modeling the inlet and outlet devices. The specification of the assembly, the



CAD model as well as the definition of the analyzed experiment is given in Table 5.3. An experiment with mixed convection condition has been selected for code validation ( $Re=20200$ ,  $Ri=5$ ). The modeling strategy involves the application of the numerical model described in Chapter 4.2, the treatment of boundary layers with industrial meshes as described in Chapter 5.1 and the validation of the hydraulic modeling as described in Chapter 5.2.1. When using an axial expansion factor of four, the mesh contains about 6 Million tetrahedrons (12 Million calculation points for the used discretization). A steady state solution was found for a simulation time which corresponds to two traverses of the calculation domain.

In the heated zone, a constant heat flux of integrally 300 kW is imposed on the outer surfaces of the rods. The same temporally and spatially constant heat flux density is imposed on each rod independently from its axial and radial localization.

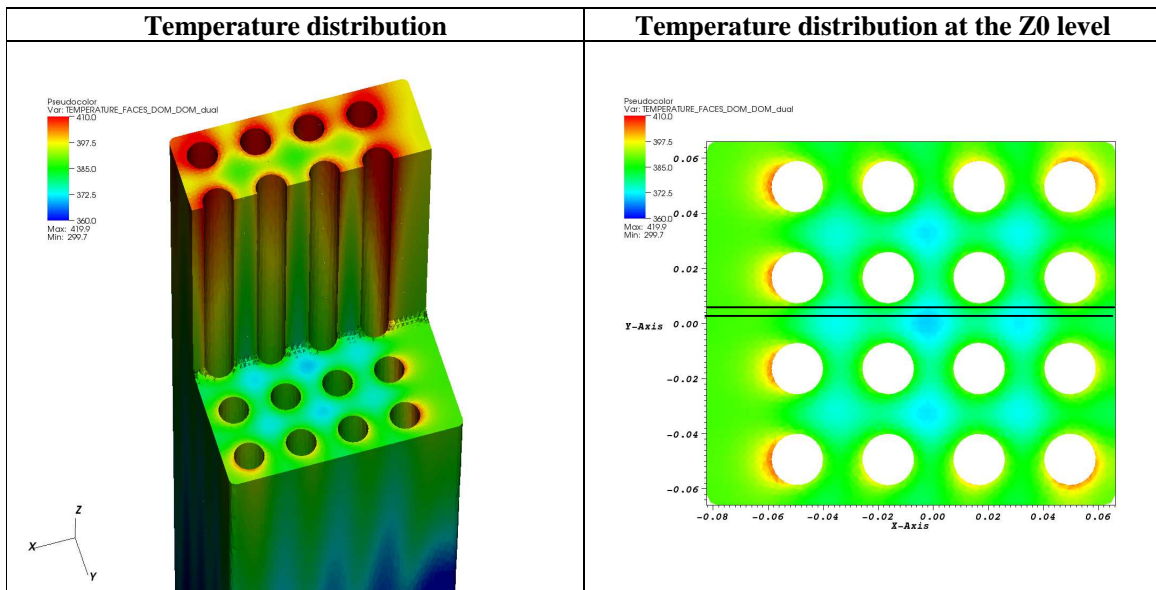


Fig. 5.8: Stationary temperature field in perspective view and in a vertical cut plane

The steady state temperature field is shown in Figure 5.8 in a perspective view and in a horizontal cut plane in the Z0 level. The domain, shown in a perspective view, is truncated at the end of the heated zone and in a vertical cut in the Z0 level. As a consequence of the injected energy, the fluid mean temperature increases from 302°C to 412.5°C with a maximum temperature attained in the peripheral sub channels.

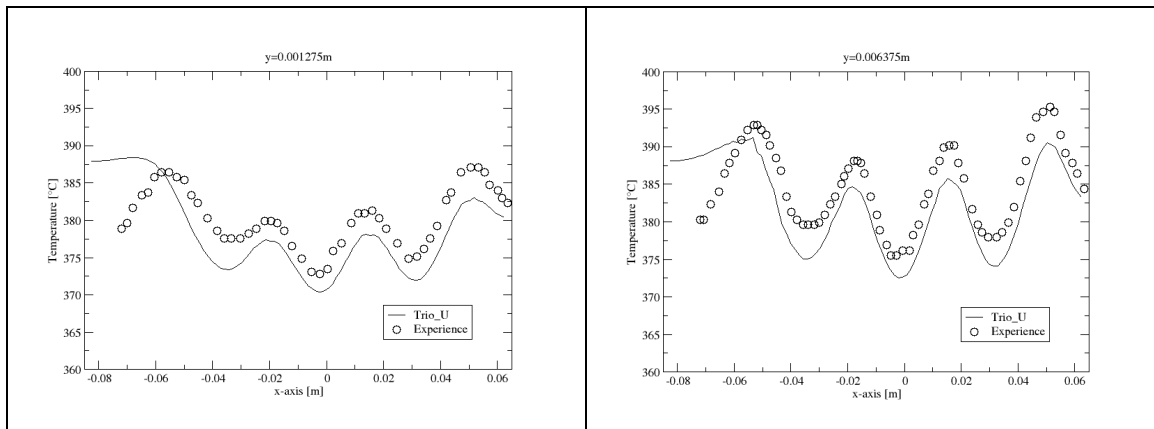


Fig. 5.9: Comparison of the measured and calculated temperature distribution



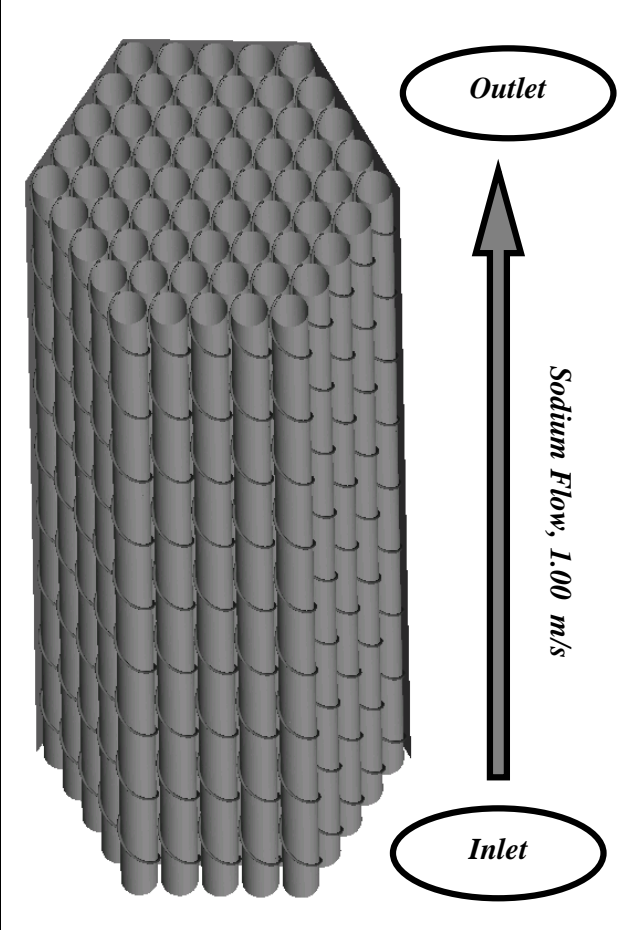
The quantitative comparison of measured and calculated temperature profiles in the Z0 level is shown in Figure 5.9. Two horizontal profiles in x direction, each at constant y abscises, are shown. The location of the profiles in the central sub channels is added to Figure 5.8. Both profiles show a good agreement between GR16 experiment and Trio\_U calculation. The calculation underestimates globally the experimental profile by 2°C. Larger difference exist in the predicted temperature in the wider sub channel at x=-0.084m. Investigations are under way to understand this behavior (probably the modeling of the outflow).

## 6 FULL SCALE FUEL ASSEMBLY

The prediction of hot spots in fuel assemblies (axially developing flow) is of major interest for reactor safety. It requires the simulation of the whole assembly. The thermal load of a full scale 61-pin wire-wrapped fuel assembly of the PHÉNIX reactor (fertile blanket) under hypothetical non uniform thermal conditions has been analyzed by using the Trio\_U code. Retaining the mesh refinement presented in Chapter 3.3 (about 150,000 tetra per rod and wire pitch and using an axial expansion factor of four), the aimed full scale rod bundle (nine wire pitches on 61 pins) needs approximately 82 Million tetrahedrons or about 170 Million calculation points. Such a mesh can not be created with the commercial mesh generators available at CEA. Thus a high quality meshing of only one wire pitch with periodic faces in flow direction (master mesh) was created with CENTAURsoft (CENTAURsoft, 2010). This master mesh has been reproduced nine times and then gathered within Trio\_U to build the final mesh of nine wire pitches.

Table 6.1: Characterization of the assembly and of the hypothetical thermal hydraulic situation

<u>Specification of the Assembly</u>	
Number of Pins	61
Diameter of Pin	13.4 [mm]
Pin Array Pitch	14.57 [mm]
Diameter of Spacer Wire	1.08 [mm]
Total Length of Pin	1800 [mm]
Length of Heated Region	1680 [mm]
Wire-wrapping Pitch	200 [mm]
<u>Experimental Conditions</u>	
Flow Rate	190 [l/min]
Total Power	442 [kW]
Inlet Temperature	450 [°C]
Average Velocity	1.00 [m/s]
Reynolds Number	8660



The specification of the assembly, the CAD model as well as the definition of the analyzed hypothetical thermal situation is given in Table 6.1.

The radial and normalized axial power distributions within the fertile blanket and in a single rod, respectively, are given in Figure 6.1 (radial power in W/cm). The fertile blanket is assumed to be located next to an experimental device with a central test channel (DAC). In the analyzed case, the DAC test channel contains light atoms which can decelerate neutrons. These neutrons, in their turn, might interact with the fuel atoms in the fertile blanket. An inhomogeneous power distribution in the fertile assembly can thus be the consequence of the presence of light atoms in the DAC.

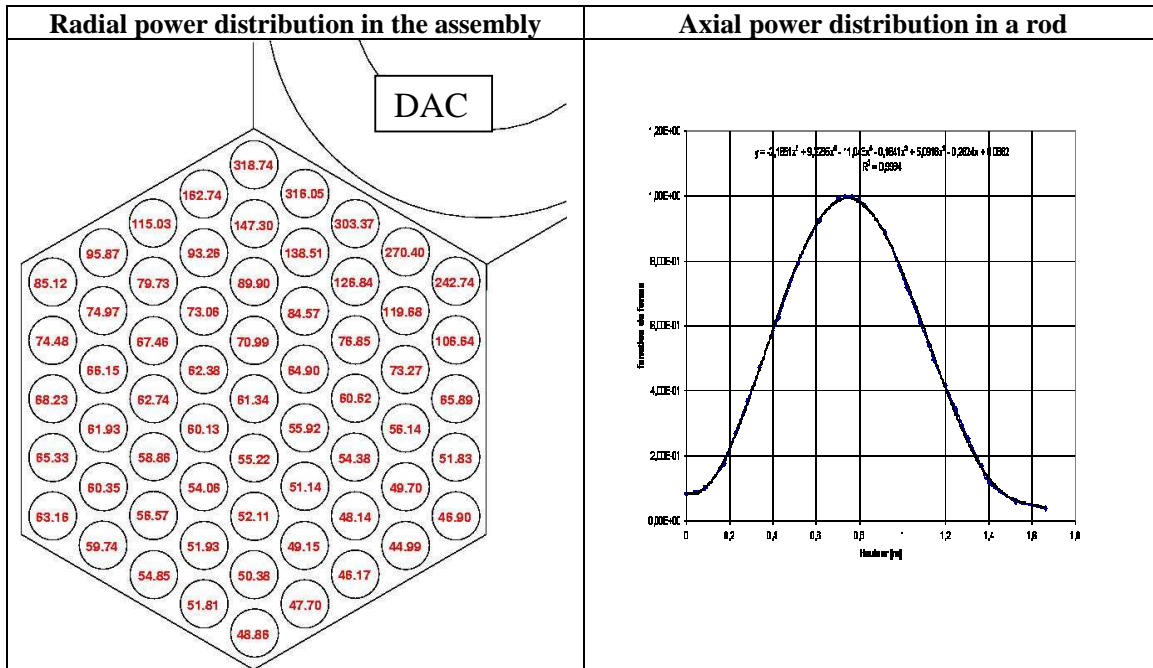


Fig. 6.1: Radial and normalized axial power distribution in the assembly

The radial distribution has been predicted by three-dimensional ERANOS calculations (ERANOS, 2008) which lead to a total power of 442 kW. An equivalent axial power distribution is applied to all rods.

The inhomogeneous temperature distribution in the fertile assembly was calculated by Trio\_U for steady state conditions. The calculation has been performed in 10 days of CPU on up to 3000 processors. The modeling strategy involves the application of the numerical model described in Chapter 4.2, the treatment of boundary layers with industrial meshes as described in Chapter 5.1 and the validation of the hydraulic and thermal-hydraulic modeling as described in Chapter 5.2.1 and 5.2.3, respectively. This procedure leads to the qualified model which now allows the prediction of thermal hydraulic phenomena in real, full scale geometries.

The predicted temperature distribution is shown in Figure 6.2 in a perspective view and for a vertical cut plane at  $x=-0.1m$ . The effect of the wire spacer in the temperature distribution is well visible in the perspective view. It is also visible, that the maximum temperature is not achieved at the assembly outlet, as in the homogeneously heated case of the PLANDTL experiment (Chapter 5.2.2) but at about 0.5m downstream of the location of maximum thermal power (at about 78% of the total length of the heated zone). This displacement is related to the mixing of the hot fluid near the DAC with the cool fluid on the opposite side of the DAC.

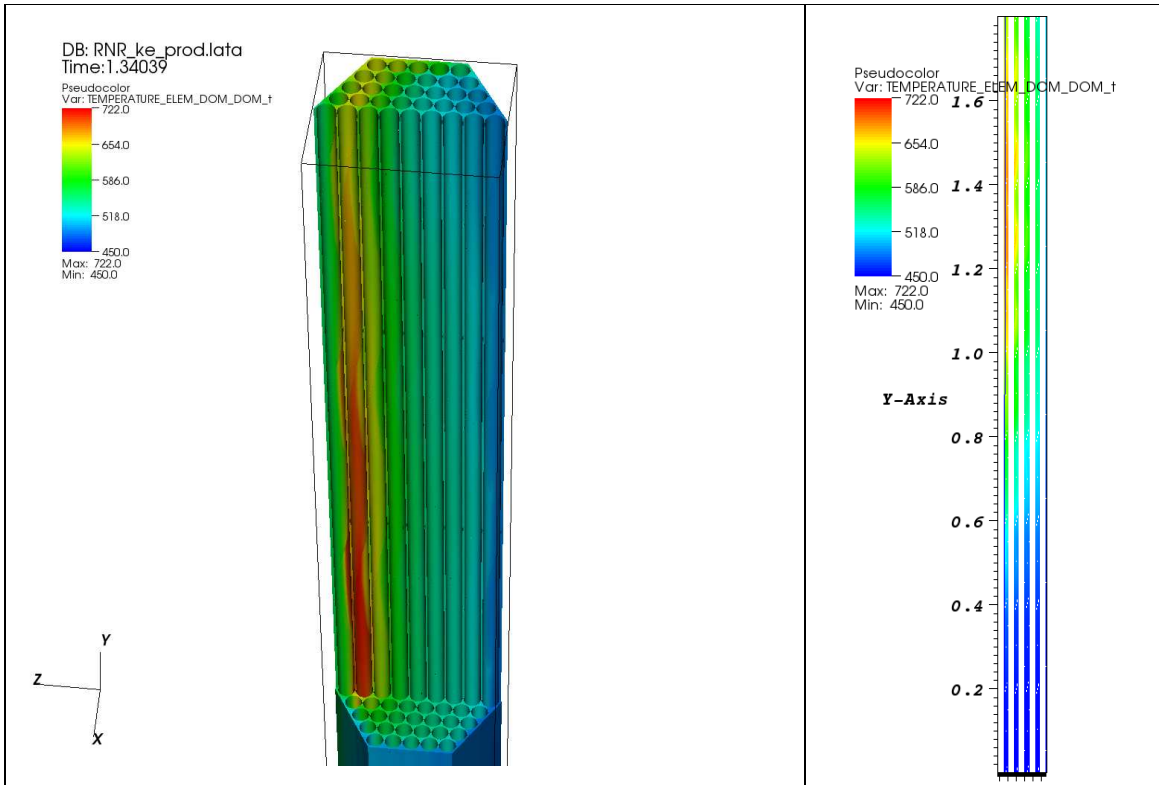


Fig. 6.2: Predicted inhomogeneous temperature distribution in the assembly

This temperature difference is illustrated in more detail in Figure 6.3, where axial temperature profiles in two sub channels are compared; one for the centre of the assembly and one near the DAC. The sinusoidal course of the temperature in the central sub channel beyond the maximum thermal power is related to the mixing of hot and cold fluid induced by the mixing wire.

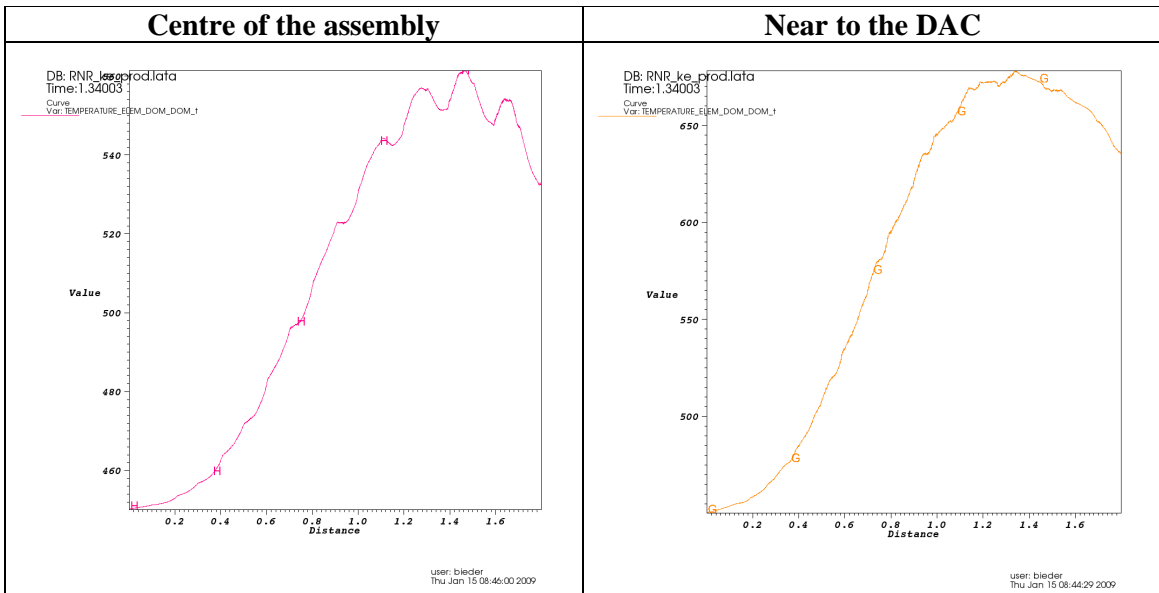


Figure 6.3: Axial temperature profiles in different sub channels

## 7 CONCLUSION

In the past, extensive numerical thermal-hydraulic investigations have been performed on the coolant of LMFBR fuel assemblies. These investigations have usually been limited to 7 to 19 wire wrapped pins and axially periodic boundary conditions due to the lack of available computer power. A modeling and validation strategy has been accomplished at CEA-Grenoble in order to analyze the thermal-hydraulic behavior of full scale, helical wrapped fuel bundles by respecting as far as possible the recommendations of Best Practice Guidelines.

The proposed validation strategy was designed for a correct prediction of the pressure and temperature field within the bundle. Validation calculations on meshes which are similar to that of the final full scale calculation and by using the same numerical modeling have been performed with a stepwise increase of the complexity of the geometry and the incorporated flow phenomena:

- Temperature development in straight tubes,
- Pressure distribution in isothermal rod bundles with wire spacers,
- Temperature distribution rod bundles with wire spacers.

Concerning the meshing, it was concluded that tetrahedral meshes with at least seven calculation points between adjacent rods are sufficient to get the pressure distribution correctly. The wall temperature with this kind of mesh might be under-predicted by at most 15%.

A critical review of existing pressure loss correlation and their usefulness for code validation has shown that it seems preferable to analyze high quality, detailed experimental data rather than using general pressure loss correlations. The axial, horizontal and azimuthal pressure distribution within a 16 pin rod bundle was predicted in good accordance to such a high quality experiment (Lafay experiment of CEA-Grenoble).

Concerning the prediction of thermal effects, the temperature distribution near the end of the heated zone of a 4x4 test bundle without wire spacers has been calculated. The calculated horizontal temperature profiles in the central sub-channels are in good accordance to data of the GR16 Sodium experiment, performed at CEA-Grenoble.

Finally, by using the validated model, the temperature distribution within a full scale 61-pin fuel assembly of 9 axial helical wire pitches of an assembly of the Phénix reactor was predicted. Generic, inhomogeneous heating conditions of a fertile blanket, located in the vicinity of an experimental test device (DAC), were assumed. The hottest region within the bundle was predicted within the heated zone, horizontally in the vicinity of the DAC and axially at approximately 78% of the total length of the heated zone.

## REFERENCES

Bertoux M., B. Menant, 1992.

Tube Bundle Detailed Thermal Hydraulics on GR16 Sodium Experiment

5<sup>th</sup> Int. Top. Meet. on Nucl. Reac. Therm. Hyd. (NURETH-5), 21-24 Sept, Salt Lake City

Berthoux M., 1995.

Interpretation of Sodium Tests in GR16 Tube Bundle using Trio\_VF Thermal-hydraulic Code.

8<sup>th</sup> IAHR Working Group Meeting on Advanced Nuclear Reactor Thermal Hydraulics,  
13-15 June, Prag, Czch. Rep.

- Berthoux, M., Carenza, A., 2008.  
 Pressure loss and heat exchange in a rod bundle representative of ETDR start-up core ESTHAIR experiment in hot air similarity.  
 The 7th International Topical Meeting on Nuclear Reactor Thermal Hydraulics, Operations and Safety (NUTHOS-7), Seoul, Korea, October 5–9.
- Bieder U., Graffard E., 2008.  
 Qualification of the CFD code Trio\_U for full scale reactor applications  
 Nuclear Engineering and Design, 238, 3, Pages 671-679
- Bubelis E., M. Schikorr, 2008  
 Review and proposal for best fit of wire-wrapped fuel bundle friction factor and pressure drop predictions using various existing correlations  
 Nuclear Engineering and Design, 238, 12, 3299-3320
- Chun M.-H., Seo K.-W., 2001.  
 An experimental study and assessment of existing friction factor correlations for wire wrapped fuel assemblies.  
 Annals of Nuclear Energy 28, 1683-1695
- CENTAURsoft, 2010.  
[www.centaurosoft.com](http://www.centaurosoft.com)
- Ducros F., U. Bieder, O. Cioni, T. Fortin, B. Fournier, G. Fauchet and P. Quéméré, 2010  
 Verification and validation considerations regarding the qualification of numerical schemes for LES for dilution problems  
 Nuclear Engineering and Design xxx (2010) xxx–xxx (online available)
- ERANOS, 2008.  
[http://den-dans.extra.cea.fr/Phocea/Vie\\_des\\_labos/Ast/ast\\_technique.php?id\\_ast=371](http://den-dans.extra.cea.fr/Phocea/Vie_des_labos/Ast/ast_technique.php?id_ast=371)
- Fernandez y Fernandez E., Carajilescov P., 2000  
 Static Pressure and Wall Shear Stress Distributions in Air Flow in a Seven Wire-Wrapped Rod Bundle  
 J. Braz. Soc. Mech. Sci. vol.22 n.2 Campinas  
[http://www.scielo.br/scielo.php?script=sci\\_arttext&pid=S0100-73862000000200012](http://www.scielo.br/scielo.php?script=sci_arttext&pid=S0100-73862000000200012)
- Gajapathy R., K. Velusamy, P. Selvaraj, P. Chellapandi, S.C. Chetal, 2009.  
 A comparative CFD investigation of helical wire-wrapped 7, 19 and 37 fuel pin bundles and its extendibility to 217 pin bundle  
 Nuclear Engineering and Design, 239, 2279–2292
- Gajapathy R., K. Velusamy, P. Selvaraj, P. Chellapandi, S.C. Chetal, 2007  
 CFD investigation of helical wire-wrapped 7-pin fuel bundle and the challenges in modeling full scale 217 pin bundle  
 Nuclear Engineering and Design, 237, 2332–2342
- Hamman K.D., R.A. Berry, 2010.  
 A CFD simulation process for fast reactor fuel assemblies  
 Nuclear Engineering and Design xxx (2010) xxx–xxx (online available)
- Lafay, J., Menant, B. and Barroil, J., 1975  
 Local pressure measurements and peripheral flow visualization in a water 19-rod bundle compared with FLICA II B calculations: influence of helical wire-wrap spacer system, AIChE/ASME Heat Transfer Conf., Paper 75-HT-22

Mahaffy J., et al. 2007.  
Best practice Guidelines for the Use of CFD in Nuclear Safety Applications  
NEA/CSNI/R(2007)5  
<http://www.nea.fr/html/nsd/docs/2007/csni-r2007-5.pdf>

Raza W., K.-Y. Kim, 2008.  
Effects of wire-spacer shape in LMR on thermal-hydraulic performance.  
Nuclear Engineering and Design, 238, 2678–2683

Smith B., et al., 2008.  
Assessment of CFD for Nuclear Reactor Safety Problems.  
NEA/CSNI/R(2007)13  
<http://www.nea.fr/html/nsd/docs/2007/csni-r2007-13.pdf>

Trio\_U, 2010.  
<http://www-trio-u.cea.fr/>